IEEE Access
Multidisciplinary | Rapid Review | Open Access Journal

Received 3 June 2022, accepted 24 June 2022, date of publication 18 July 2022, date of current version 21 July 2022.

Digital Object Identifier 10.1109/ACCESS.2022.3188444

RESEARCH ARTICLE

Novel Multiplexing Scheme for Resolving the Velocity Ambiguity Problem in MIMO FMCW Radar Using MPSK Code

JEONG-HOON PARK[1,2], (Graduate Student Member, IEEE), YOUNG-JUN YOON[1,2], (Graduate Student Member, IEEE), JAEHOON JUNG[1,2], (Graduate Student Member, IEEE), AND SEONG-CHEOL KIM[1,2], (Senior Member, IEEE)

[1]Department of Electrical and Computer Engineering, College of Engineering, Seoul National University (SNU), Seoul 08826, Republic of Korea
[2]College of Engineering, Institute of New Media and Communications (INMC), Seoul National University (SNU), Seoul 08826, Republic of Korea

Corresponding author: Seong-Cheol Kim (sckim@maxwell.snu.ac.kr)

This work was supported by Samsung Electronics Company Ltd., under Grant IO210202-08366-01.

ABSTRACT For the high-resolution DoA (Direction of Arrival) estimation, various multiplexing schemes are considered for the multi-input multi-output (MIMO) fast chirp frequency-modulated continuous-wave (FMCW) radar. However, current schemes such as time-division multiplexing (TDM) and binary-phase modulation (BPM) may reduce the maximum detectable velocity, which causes the velocity ambiguity problem. As an extension of the BPM scheme to mitigate this issue, we propose a novel multiplexing scheme using M phase-shift keying (MPSK) code which duplicates shifted target peaks at unequal intervals over the velocity domain. The proposed scheme finds the true peaks to resolve the velocity ambiguity problem by the inversion of the circulant matrix with low additional computation. In addition, the successful implementation of the proposed scheme is conducted with 4 by 8 MIMO uniform linear array (ULA) antennas through the state-of-the-art FMCW radar. Finally, the proposed scheme is compared to the conventional TDM based MIMO scheme regarding signal to noise ratio (SNR) and phase calibration issues for moving targets. The proposed scheme is to estimate the accurate 4D information of targets while resolving the velocity ambiguity problem in the MIMO FMCW radar systems.

INDEX TERMS FMCW, MIMO, MPSK code, velocity ambiguity, DoA estimation.

I. INTRODUCTION

Heading towards the era of autonomous driving systems, the fast chirp frequency-modulated continuous-wave (FMCW) radar is widely used as an important sensor for its reliable and cost-effective advantages [1]–[3]. With its ability to obtain 4D information (i.e., range, velocity, azimuth, and elevation angle) of targets, it can localize the target and construct its image for reliable autonomous driving [4], [5]. Above all, one of the most challenging issues is enhancing angle estimation performance which requires multiple receiving (Rx) antenna elements [6], [7]. However, the increased number of Rx antenna elements leads to higher cost and excessive antenna aperture size, resulting in additional design difficulties.

As a solution to the forementioned issues, the multi-input multi-output (MIMO) antenna array with various multiplexing schemes can be applied to chirp units [8]. Various multiplexing schemes for the MIMO radar, such as time-division multiplexing (TDM) [9], [10], code-division multiplexing (CDM) [11], [12], and frequency division multiplexing (FDM) [13], ensure orthogonality between Tx signals so that they can be separated in each Rx signal. Consequently, the MIMO antenna array with N_{Tx} Tx antenna elements and N_{Rx} Rx antenna elements can be configured to a virtual antenna array with a single Tx antenna element and $N_{\mathrm{Tx}}N_{\mathrm{Rx}}$ virtual Rx antenna elements.

The associate editor coordinating the review of this manuscript and approving it for publication was Chengpeng Hao.

However, the main problem of the MIMO antenna array with the above multiplexing schemes is that the maximum detectable velocity decreases in proportion to N_{Tx}. Since the state-of-the-art 4D imaging radar uses tens of Tx antenna elements as listed in Table. 1, it leads to severe velocity ambiguity problems which can be detrimental to autonomous driving systems.

To solve the forementioned velocity ambiguity problem, some previous works used different chirp configurations with different maximum detectable velocities to estimate the exact velocity of the target using the Chinese remainder theorem [17] or clustering algorithms [18]. However, small velocity estimation errors for different chirp configurations make it hard to determine the exact velocity of the target, which is inevitable in real scenarios. Another method using the hypothetical phase compensation(HPC) based on the TDM scheme [19] determined the target's velocity by selecting the velocity with the best angle estimation performance. However, it requires additional angle estimation for each hypothetical velocity and tends to show unstable performance. Furthermore, both methods cannot fully use all the time slots, which leads to the reduction of signal to noise ratio (SNR) or frame per second (FPS).

Since the CDM scheme can fully use all the time slots and can solve the above stability issues, our approach focuses on the CDM scheme to resolve the velocity ambiguity problem. Existing CDM based schemes use binary phase modulation (BPM) to resolve the velocity ambiguity problem by comparing the power of each peak to separate Tx signals [20], [21]. However, different radar channels between each Tx-Rx pair cause another ambiguity in distinguishing each peak. In [21], peaks replicated by binary codes are matched to each Tx antenna element, and angle estimations are performed for all possible matchings. However, this method requires significant amount of computation, especially when N_{Tx} increases. To mitigate the above issues in BPM, the M phase-shift keying (MPSK) code for the MIMO radar was first proposed in [22]. This method finds an arithmetic sequence of the phase of each peak to separate Tx signals. However, due to phase distortion caused by reflected signal's incoherency and hardware issues, this method becomes more vulnerable to errors as N_{Tx} increases. Therefore, the feasibility of the MIMO FMCW radar using the MPSK code to resolve the velocity ambiguity problem still remains questionable.

As a robust solution to the velocity ambiguity problem in the MIMO FMCW radar using the MPSK code, we propose a novel multiplexing scheme assigning a MPSK code to the chirp-sequence which shifts target peaks with unequal intervals over the velocity domain. Regardless of the phase distortion and the computation complexity issues in the previous methods, the proposed scheme was successfully implemented with the state-of-the-art FMCW radar evaluation kit. Furthermore, we showed that the proposed scheme has various advantages over the conventional TDM scheme. Along with the advantage of resolving the velocity ambiguity problem, the proposed scheme showed higher SNR properties and more accurate angle estimation performance for moving targets compared to the TDM based MIMO radar.

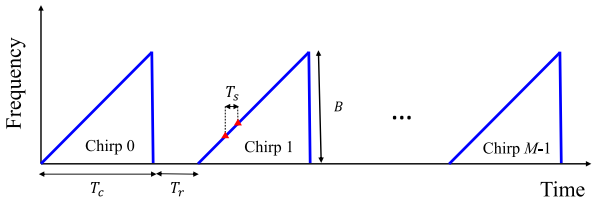

FIGURE 1. Basic signal structure of FMCW radar.

The remainder of this paper is organized as follows. First, the range, velocity and angle estimation of the FMCW radar system is introduced in Section II. In Section III, Multiplexing schemes for the MIMO FMCW radar to enhance DoA estimation are presented. In addition, related works to resolve the velocity ambiguity problem for the MIMO FMCW radar are presented. In section IV, the novel multiplexing scheme assigning a specific MPSK code for each chirp-sequence is proposed with simulation results. Consequently, the implementation of the proposed scheme using a commercial radar and performance comparisons with the TDM scheme are shown in Section V. Finally, conclusions are provided in Section VI.

II. SYSTEM MODEL

In this paper, the fast chirp FMCW radar system is considered. The received signals of the single-input multi-output (SIMO) array from the targets are modeled and the corresponding range, velocity and angle estimation schemes are introduced.

Fig. 1 shows the basic structure of the fast chirp FMCW radar signal. One signal frame of the FMCW radar consists of M (an even number) repeating chirp signals, whose frequency increases linearly with time. The transmitted signal of each chirp with time t can be expressed as

$$s(t) = \exp\left\{j2\pi\left(f_c t + \frac{B}{2T_{\mathrm{c}}}t^2\right)\right\} \mathrm{rect}\left(\frac{T_{\mathrm{c}} - t}{T_{\mathrm{c}}}\right), \tag{1}$$

where c, f_{c}, B, and T_{c} denote the speed of light, the carrier frequency, the bandwidth, and the duration of the chirp signal. $\mathrm{rect}(\cdot)$ indicates the rectangular shaping filter expressed as

$$\mathrm{rect}(u) = \begin{cases} 1, & \text{if } 0 < u < 1 \\ 0, & \text{otherwise.} \end{cases} \tag{2}$$

If we assume the maximum delay from the target which is located at distance R from the radar is smaller than the chirp rest time T_{r} ($i.e\ \frac{2R}{c} < T_{\mathrm{r}}$), the received signal of the m-th chirp reflected from a single target with the distance of R and the radial velocity of v can be expressed as

$$s_r^m(t) = s\left(t - \frac{2(R + v(m(T_{\mathrm{r}} + T_{\mathrm{c}}) + t))}{c}\right). \tag{3}$$

After mixing the transmitted signal and the received signal, and passing through the low pass filter, the continuous signal

TABLE 1. Number of Tx antenna elements for various 4D imaging radar.

Model	Retina 4F [14]	MMWCAS-RF-EVM [15]	XRR chip [16]
Company	Smart Radar System	Texas Instrument	Vayyar
N_{Tx}	12	12	48
Year of release	2021	2020	2021

is converted to the discrete signal with N samples per chirp (*i.e* sampling time $T_{\mathrm{s}} = T_{\mathrm{c}}/N$). Then, we can obtain the discrete beat signal

$$s_b[n,m] = \exp\left\{j2\pi\left(\frac{2RB}{T_{\mathrm{c}}c}nT\mathrm{s} + \frac{2f_{\mathrm{c}}v}{c}m(T_{\mathrm{c}}+T_{\mathrm{r}}) + \phi\right)\right\} \quad (n=0,1\cdots N-1, m=0,1\cdots M-1), \tag{4}$$

where $s_b[n,m]$ and ϕ denote the n-th sample of the beat signal at the m-th chirp and a constant phase component.

A. RANGE-VELOCITY ESTIMATION

The range of the target is estimated with the delay of the signal reflected from the target. Since mixing the Tx and Rx signals generates the first phase term in the exponent as given in (4), linearly increasing phases over the samples can be obtained for a given chirp index. Similarly, the velocity of the target is estimated through the phase shift over the chirps due to the target's motion. As given in (4), linearly increasing phases over the chirps proportional to the target's velocity can be obtained for a given sample index. Based on these properties, the range-velocity profile of the target can be obtained by applying 2-D Fourier transform to $s_b[n,m]$ as shown in Fig. 2. As we denote the sample index and the chirp index of the resulting peak as $(\widehat{n},\widehat{m})$, the range and velocity of the target can be achieved by

$$R = \frac{c}{2B}\widehat{n}$$
$$v = \begin{cases} \dfrac{c}{2Mf_{\mathrm{c}}(T_{\mathrm{c}}+T_{\mathrm{r}})}\widehat{m}, & \text{if } 0 \le \widehat{m} \le [\dfrac{M}{2}] \\ \dfrac{c}{2Mf_{\mathrm{c}}(T_{\mathrm{c}}+T_{\mathrm{r}})}(\widehat{m}-M), & \text{otherwise,} \end{cases} \tag{5}$$

where $[\cdot]$ indicates gaussian function where $[x]$ is the largest integer not greater than x. Note that the estimated velocity's denominator term has a factor of 2 to be able to return a positive or negative velocity value. The resolution of the range and velocity are determined by the interval between two adjacent estimated values in (5). In addition, the maximum detectable range and velocity are determined by the (5) when $\widehat{n}=N$ and $\widehat{m}=\frac{M}{2}$. In short, it can be written as

$$R_{\mathrm{res}} = \frac{c}{2B},\quad R_{\mathrm{amb}} = \frac{cN}{2B}$$
$$v_{\mathrm{res}} = \frac{c}{2Mf_{\mathrm{c}}(T_{\mathrm{c}}+T_{\mathrm{r}})},\quad v_{\mathrm{amb}} = \frac{c}{4f_{\mathrm{c}}(T_{\mathrm{c}}+T_{\mathrm{r}})}, \tag{6}$$

where R_{res}, R_{amb}, v_{res}, and v_{amb} represent the range resolution, the maximum detectable range (ambiguous range), the velocity resolution, and the maximum detectable velocity (ambiguous velocity), respectively.

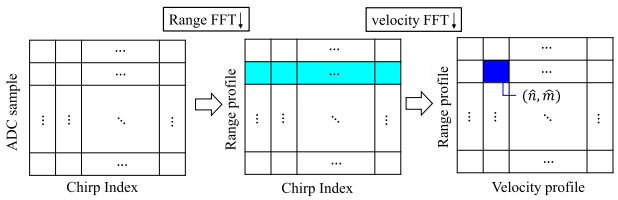

FIGURE 2. R-v estimation of FMCW radar.

B. ANGLE ESTIMATION USING SIMO ARRAY

In this section, a SIMO array with one Tx antenna element and multiple Rx antenna elements is considered as depicted in Fig 3. Assume that the target is located at an angle of θ from the radar and d represents the spacing between two adjacent Rx antenna elements. Since the received signal reflected from the target has a constant phase difference $\frac{d\sin(\theta)}{\lambda}$ (λ: wavelength of the radar signal) between two adjacent Rx antenna elements, Rx signal for each Rx antenna element can be expressed as

$$s_b[n,m,k] = \exp\left\{j2\pi\left(\frac{2RB}{T_{\mathrm{c}}c}nT\mathrm{s} + \frac{2f_{\mathrm{c}}v}{c}m(T_{\mathrm{c}}+T_{\mathrm{r}}) + \frac{d\sin(\theta)}{\lambda}k + \phi\right)\right\} \quad (n=0,1\cdots N-1, m=0,1\cdots M-1, k=0,1\cdots N_{\mathrm{Rx}}-1), \tag{7}$$

where k denotes Rx antenna element index. Similar to R-v estimation process, Fourier transform can be applied over Rx antenna index k to estimate the target's angle θ. Furthermore, multiple signal classification (MUSIC) can be used to improve the angle estimation performance by separating the noise subspace and the signal subspace [1], [23], [24]. In this paper, MUSIC is used to examine the DoA estimation performance of the proposed scheme and more specific descriptions will be given in the following section.

III. MULTIPLEXING SCHEME FOR MIMO RADAR

For high-resolution DoA estimation, more Rx antenna elements are required. The virtual antenna array with a single Tx antenna element and multiple Rx antenna elements is configured by separating Tx signals. In this section, we introduce how to configure a virtual array for the MIMO system under the assumption that Tx signals are to be separated. In addition, we introduce more specific descriptions of the existing TDM and CDM schemes and effective methods to separate Tx signals in both schemes.

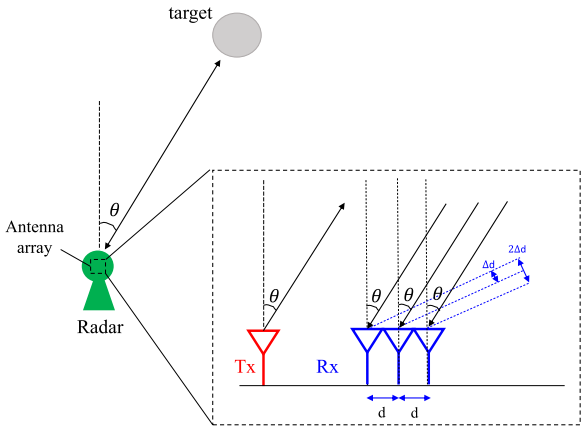

FIGURE 3. Angle estimation of FMCW radar with a SIMO array.

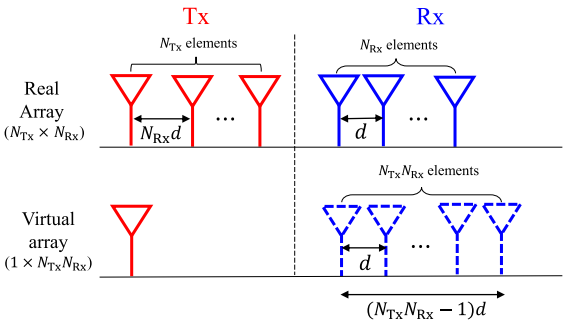

FIGURE 4. Virtual array configuration.

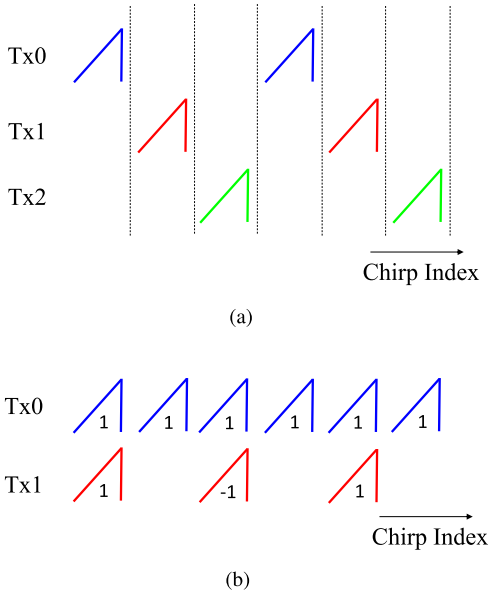

FIGURE 5. Example of the multiplexing scheme (a) TDM (b) BPM.

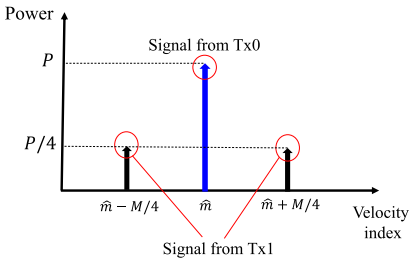

FIGURE 6. Detected peaks with an orthogonal code in [20].

A. VIRTUAL ARRAY CONFIGURATION FOR MIMO SYSTEM

Fig. 4 shows the real and virtual antenna array configurations. $N_{\mathrm{Tx}} \times N_{\mathrm{Rx}}$ MIMO ULA was considered. The spacing between two adjacent Rx and Tx antenna elements are set to be d and $N_{\mathrm{Rx}}d$, respectively.

Since the phase difference of the received signal between two adjacent Rx antenna elements is $\frac{d \sin\theta}{\lambda}$, and the phase difference between two adjacent Tx antenna elements is equal to $N_{\mathrm{Rx}}\frac{d \sin\theta}{\lambda}$, the signal from the i-th Tx to the j-th Rx has a phase difference of $(iN_{\mathrm{Rx}} + j)\frac{d \sin\theta}{\lambda}$ with respect to the 0-th Tx element and the 0-th Rx element. If the received signals from different Tx antenna elements are separated, all phase differences from 0 to $(N_{\mathrm{Rx}}N_{\mathrm{Tx}} - 1)\frac{d \sin\theta}{\lambda}$ can be obtained by interval of $\frac{d \sin\theta}{\lambda}$. In other words, it is equivalent to receive $N_{\mathrm{Tx}}N_{\mathrm{Rx}}$ signals with uniform phase difference of $\frac{d \sin\theta}{\lambda}$. Hence, a $N_{\mathrm{Tx}} \times N_{\mathrm{Rx}}$ MIMO array can be configured as an $1 \times N_{\mathrm{Tx}}N_{\mathrm{Rx}}$ SIMO virtual array.

B. TIME DIVISION MULTIPLEXING (TDM)

The most widely used multiplexing scheme for the MIMO radar is known to be the TDM scheme, which divides time slots and allocates them to different Tx antenna elements alternately. For example, 3 Tx antenna elements alternately transmitting signals in different time slots are shown in Fig. 5(a). Since the received signal from different Tx antenna elements can be separated by reconstructing each time slot signal, the TDM scheme is simple to implement and guarantees ideal orthogonality [7].

However, the TDM scheme has a major disadvantage that the maximum detectable velocity reduces by $1/N_{\mathrm{Tx}}$ times. This is because the time interval $(T_{\mathrm{c}} + T_{\mathrm{r}})$ between two consecutive chirps increases by N_{Tx} times due to alternate transmissions in N_{Tx} time slots. Therefore, referring to Equation 6, the maximum detectable velocity (v_{amb}) reduces by $1/N_{\mathrm{Tx}}$ times, which is a severe problem in the TDM MIMO scheme.

C. CODE DIVISION MULTIPLEXING (CDM)

Unlike the TDM scheme, the CDM scheme fully use all the time slots by assigning an orthogonal code for the chirp-sequences. For example, Fig. 5(b) shows the CDM scheme with the binary phase modulation(BPM) that repeats $[1\ 0\ -1\ 0]$ binary code for Tx1. Since Tx0 transmits the signal in every time slots, it ensures more transmitting power. Therefore, the CDM scheme can enhance SNR by N_{Tx} times than

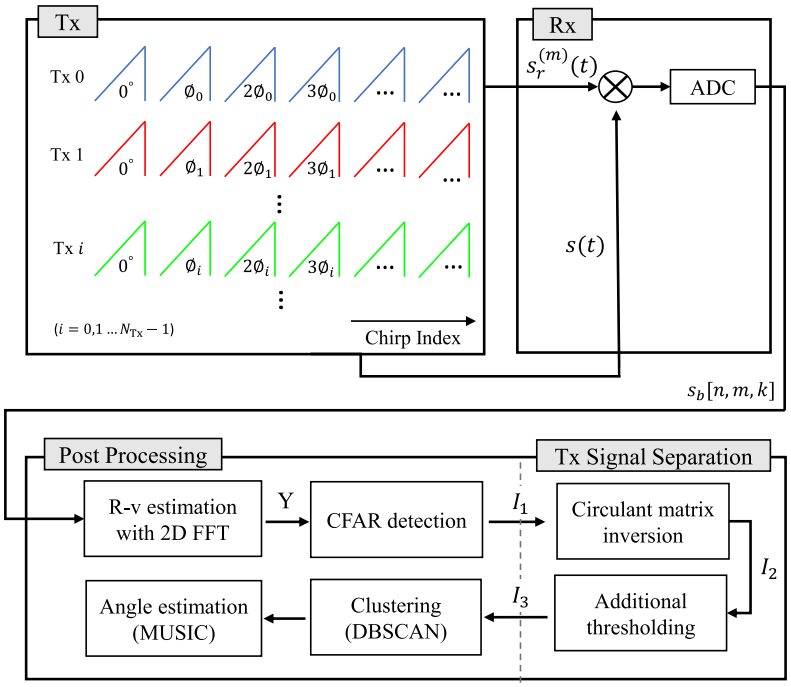

FIGURE 7. Processing for the proposed multiplexing scheme.

the TDM scheme. However, the repetition of an orthogonal code in the CDM scheme still causes the reduction of the maximum detectable velocity. Since the detected target peaks over the velocity domain include the ghost target peaks due to the repetition of an orthogonal code, the true target peaks should be found to solve the velocity ambiguity problem.

To overcome this issue, authors in [20] used the binary phase modulation that repeats the [1 0 −1 0] binary code for Tx1 as shown in Fig. 5(b). As a result, the target peak of Tx1's signal was shown to be shifted to both sides by M/4 index over the velocity domain as shown in Fig. 6 and the highest peak was determined as the true peak. Similarly, binary phase modulation with Hadamard code was used in [21] and the MPSK code was used in [22]. To resolve the velocity ambiguity problem, detected target peaks including the ghost target peaks by an orthogonal code are matched to each Tx antenna element and true peaks are found. However, these methods have some limitations to implement on real device as mentioned in section 2. To overcome these issues, we propose a novel multiplexing scheme to resolve the velocity ambiguity problem and to enhance DoA estimation performance in the following section.

IV. PROPOSED MPSK CHIRP CODE BASED MULTIPLEXING SCHEME FOR MIMO RADAR

Fig. 7 shows the overall process of the proposed scheme. The proposed multiplexing scheme for the MIMO system uses the MPSK code with the phase proportional to the chirp index and multiplies it to a chirp sequence before transmission. After mixing the received signal with the transmitted signal, the mixed signal is converted into the discrete beat signal by the down-converter and the analog-to-digital converter (ADC). By the proposed post-processing for the received beat signal, Tx signals are separated in each Rx antenna element and the true velocities of the targets are estimated without the velocity ambiguity problem. Finally, DoA of the detected targets are estimated via MUSIC with a virtual antenna array. It will be explained in more detail in the following section.

A. SIGNAL MODEL

Tx signals in the proposed scheme with the MPSK code is expressed as

$$s^{(m,i)}(t) = s(t)\exp(-j2\pi m\phi_i), \tag{8}$$

where $s^{(m,i)}(t)$ denotes the m-th chirp Tx signal for the i-th Tx antenna element and ϕ_i denotes the MPSK code for the i-th Tx antenna element. In this paper, the group of MPSK code with M_{code}=16 was considered ($i.e.$ $\phi_i \in \{0, \frac{1}{16}, \frac{2}{16} \cdots \frac{15}{16}\}$). The resulting discrete beat signal in (3) is modified to

$$\begin{aligned} s_b[n, m, k] = \sum_{i=0}^{N_{\text{Tx}}-1} \exp\Bigg\{ j2\pi \Bigg(& \frac{2RB}{T_c c} n T_s \\ & + \frac{2f_c v}{c} m(T_c + T_r) - m\phi_i + \frac{d\sin(\theta)}{\lambda} k + \phi \Bigg) \Bigg\} \\ & (n = 0, 1 \cdots N-1, m = 0, 1 \cdots M-1, \\ & k = 0, 1 \cdots N_{\text{Rx}} - 1). \end{aligned} \tag{9}$$

As shown in (9), the proposed MPSK code term $j2\pi m\phi_i$ shifts the peak of the target by -$M\phi_i$ index in the velocity domain. In other words, $\widehat{m}$ in (5) is changed to $\widehat{m} - M\phi_i$ by

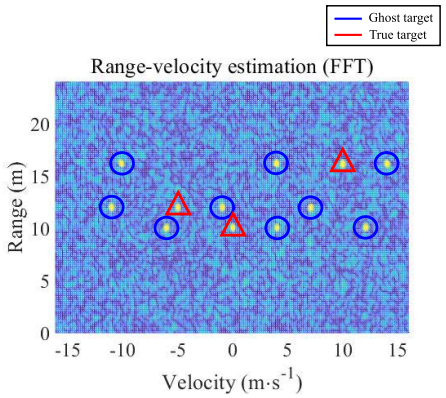

FIGURE 8. R-v estimation with the proposed scheme.

TABLE 2. Parameters and values of simulation.

Parameter	Value
Carrier frequency (f_c)	77 GHz
Bandwidth (B)	1 GHz
Duration of the chirp time (T_c)	50μs
chirp rest time (T_r)	10μs
The number of chirps in one frame M	128
The number of samples in one chirp N	256
The number of transmit antenna elements(N_{Tx})	4
The number of receiving antenna elements(N_{Rx})	8
SNR	5dB

the i-th Tx signal. For the simulation, $N_p = 3$ targets with $(R(\mathrm{m}), v(\mathrm{m/s}), \theta(\mathrm{rad})) = (10, 0, 0.2), (16, 10, -0.24), (25, -5, 0.3)$ was assumed. $N_{Tx} = 4$, $N_{Rx} = 8$ and the MPSK codes for each Tx antenna element, $\{\phi_0, \phi_1, \phi_2, \phi_3\}$ is set to be $\{0, \frac{3}{16}, \frac{10}{16}, \frac{14}{16}\}$. Parameters of the radar are specified in Table 2.

As we denote 2D FFT of s_b for the k-th Rx antenna element as Y_k, 2D FFT of the received signal for each Rx antenna element shows total 12 target peaks in the R-v domain as shown in Fig. 8. True target peaks by Tx0 without the MPSK code are marked with red triangle and the shifted ghost target peaks by the MPSK code are marked with blue circle.

For the target detection, the constant false alarm rate (CFAR) algorithm is used. CFAR is a detection technique to maintain a constant false alarm probability in a complex clutter environment [25], [26] with the thresholding factor determined by the neighboring cells. We used the 2D cell averaging (CA)-CFAR algorithm [26] which estimates the clutter power Z by averaging the training cell values. Fig. 9(a) shows a brief structure of 2D CA-CFAR. CA-CFAR with false alarm rate $(P_{fa}) = 10^{-7}$, guard band size $(N_{gx}, N_{gy}) = (2, 2)$, training band size $(N_{tx}, N_{ty}) = (6, 4)$ were used. Assuming the additive gaussian noise, the scaling factor S is determined by [27]

$$S = N_T(P_{\mathrm{fa}}^{-1/N_T} - 1), \tag{10}$$

where N_T denotes number of training cells.

With the thresholding factor $S \cdot Z$, Index_peak1 (I_1) is determined as

$$\mathrm{I}_1[n, m] = \begin{cases} 1, & \text{if } \mathrm{Y}_0[n, m] > S \cdot Z \\ 0, & \text{otherwise} \end{cases} \\ (n = 0, 1 \cdots N-1, m = 0, 1 \cdots M-1). \tag{11}$$

Index_peak1 (I_1) has the value of 1 for the cells corresponding to the detected targets, otherwise 0.

B. TRANSMITTED SIGNAL SEPARATION METHOD

To find the true target peaks among the detected peaks over the velocity domain, we used the property of the circulant matrix to separate Tx signals. If $N \times M$ matrix representing the original target peaks is denoted as O, and the matrix representing the target peaks shifted by l index in the row direction is denoted as I, the relationship between O and I can be expressed as follows

$$\mathrm{I} = \mathrm{OA}_l. \tag{12}$$

A_l denotes $M \times M$ circulant matrix [28], and the peak of the target is shifted by l index over the velocity domain by multiplying A_l. A_l can be expressed as

$$\mathrm{A}_l = \begin{bmatrix} a_0 & a_1 & \cdots & a_{M-2} & a_{M-1} \\ a_{M-1} & a_0 & a_1 & \cdots & a_{M-2} \\ \vdots & \ddots & \ddots & \ddots & \\ a_2 & a_3 & \cdots & a_0 & a_1 \\ a_1 & a_2 & \cdots & a_{M-1} & a_0 \end{bmatrix}, \tag{13}$$

where $a_i = \begin{cases} 1, \text{ if } i = l \\ 0, \text{ otherwise} \end{cases} \quad (i = 0, 1 \cdots M-1).$

Similarly, Index_peak2 (I_2) representing the cells of the true target peaks among the detected targets can be represented by Index_Peak1 and the circulant matrix as follows

$$\mathrm{I}_1 = \mathrm{I}_2\mathrm{A}, \tag{14}$$

where A denotes circulant matrix with the coefficient expressed as

$$\mathrm{A} = \mathrm{A}_{M\phi_0} + \mathrm{A}_{M\phi_1} + \mathrm{A}_{M\phi_2} + \mathrm{A}_{M\phi_3}. \tag{15}$$

Index_peak2 contains the location information of the true target cells which is red-circled in Fig. 8. As the proposed multiplexing scheme shifts target peaks by $-M\phi_i$ index over the velocity domain and the spacing between the shifted peaks are unequal, Index_peak2 can be obtained by multiplying inverse matrix of A. The invertible conditions of the circulant matrix will be discussed in the following section V. In result,

$$\mathrm{I}_2 = \mathrm{I}_1\mathrm{A}^{-1}. \tag{16}$$

To reduce the computation complexity, we notice that the circulant matrix A can be readily diagonalized by

$$\mathrm{A} = \mathrm{F}^H\mathrm{DF}, \tag{17}$$

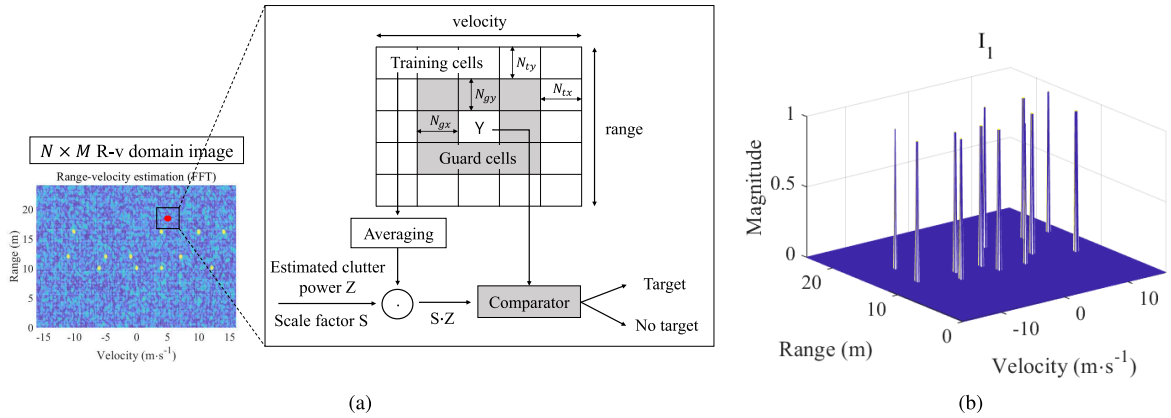

FIGURE 9. (a) Brief structure of 2D CA-CFAR algorithm, (b) the corresponding result.

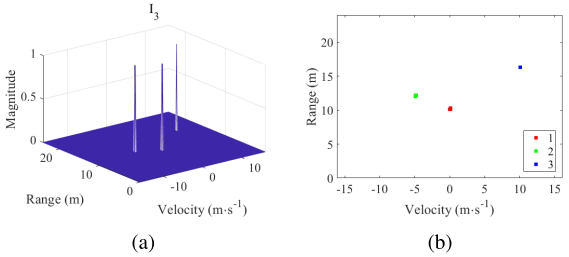

FIGURE 10. (a) Detected true target cells (I_3) (b) DBSCAN.

, where F denotes Discrete Fourier Transform (DFT) matrix and D denotes diagonal matrix [28]. Therefore, (16) can be expressed as

$$\mathrm{I}_2 = \mathrm{I}_1 \mathrm{F}^H \mathrm{D}^{-1} \mathrm{F}. \tag{18}$$

It is notable that matrix conversion in (16) has complexity of $O(Mlog(M))$ with fast Fourier transform (FFT) [29], which is more relaxed than general matrix inversion with complexity $O(M^3)$. Finally, elementwise product of I_1 and I_2 ($\mathrm{I}_1 \odot \mathrm{I}_2$) with additional thresholding factor $\theta = 0.8$ are used to filter out the noise components. For the real experiment data, additional thresholding is necessary because all radar channels for each transmitter-receiver pair are different. For example, few cells corresponding to target1 can be detected in the Tx1-Rx1 channel but not in the Tx2-Rx1 channel. With the above steps, we obtain Index_peak3 (I_3) which represents the true peaks of the targets.

$$\mathrm{I}_3[n,m] = \begin{cases} 1, & \text{if } \mathrm{I}_1[n,m] \times \mathrm{I}_2[n,m] > \theta \\ 0, & \text{otherwise} \end{cases}$$
$$(n = 0, 1 \cdots N-1, m = 0, 1 \cdots M-1). \tag{19}$$

In this simulation, Index_peak3 (I_3) shows 3 target peaks in R-v domain as shown in Fig. 10. Consequently, we applied a clustering algorithm, density-based spatial clustering of applications with noise(DBSCAN) [30] to separate the peaks and to estimate DoA for each target peak. Since the clustering is not necessary step for the proposed scheme, we will skip the specific description about DBSCAN algorithm. After the peaks of targets are clustered in R-v domain, Index_peak3 is divided according to the number of labels. As we denote the peak of the n_p-th labeled target as $\mathrm{I}_3^{(n_\mathrm{p})}$, $\mathrm{I}_3 = \sum_{n_\mathrm{p}=0}^{N_\mathrm{p}-1} \mathrm{I}_3^{(n_\mathrm{p})}$.

C. ANGLE ESTIMATION WITH VIRTUAL ARRAY CONFIGURATION

By extracting the overlapping part of I_3 and I_1, it is possible to obtain the signal from Tx0 for each Rx antenna element. Similarly, $\mathrm{I}_3\mathrm{A}_i$ instead of I_3 can be used to obtain the signal by the i-th Tx antenna element for each Rx antenna element. In result, total $N_\mathrm{Tx}N_\mathrm{Rx}$ separated signals are constructed for the virtual array. It can be written as

$$\mathrm{Q}_{i,k}^{(n_p)} = \mathrm{NZ}(\mathrm{Y}_k \odot (\mathrm{I}_3^{(n_p)} \mathrm{A}_i))$$
$$(i = 0, 1 \cdots N_\mathrm{Tx} - 1, k = 0, 1 \cdots N_\mathrm{Rx}), \tag{20}$$

where $\mathrm{Q}_{i,k}^{(n_p)}$ denotes the target peaks from the i-th Tx separated at the k-th Rx for the n_p-th labeled target. Since what we need in $\mathrm{Q}_{i,k}$ is only non-zero components, $\mathrm{NZ}(\cdot)$ operation which extracts the non-zero components of the matrix and vectorize it to the row vector was used. To estimate DoA of the n_p-th labeled target, $\mathrm{Q}_{i,k}^{(n_\mathrm{p})}$s are stacked in the column for the input signal data to the MUSIC algorithm, denoted as

$$\mathrm{X} = \begin{bmatrix} \mathrm{Q}_{0,0}^{(n_\mathrm{p})} \\ \mathrm{Q}_{0,1}^{(n_\mathrm{p})} \\ \vdots \\ \mathrm{Q}_{N_\mathrm{Tx}-1,N_\mathrm{Rx}-1}^{(n_\mathrm{p})} \end{bmatrix}. \tag{21}$$

It has the row size equal to the number of detected peak cells for the n_p-th labeled target, and the column size equal to $N_\mathrm{Tx}N_\mathrm{Rx}$. Through eigenvalue decomposition, XX^H is expressed as

$$\mathrm{XX}^\mathrm{H} = \mathrm{UDU}^\mathrm{H}, \tag{22}$$

where U is $N_\mathrm{Tx}N_\mathrm{Rx}$ unitary matrix whose column vectors are eigenvectors. D is $N_\mathrm{Tx}N_\mathrm{Rx} \times N_\mathrm{Tx}N_\mathrm{Rx}$ diagonal matrix whose components are eigenvalues in descending order. Except the

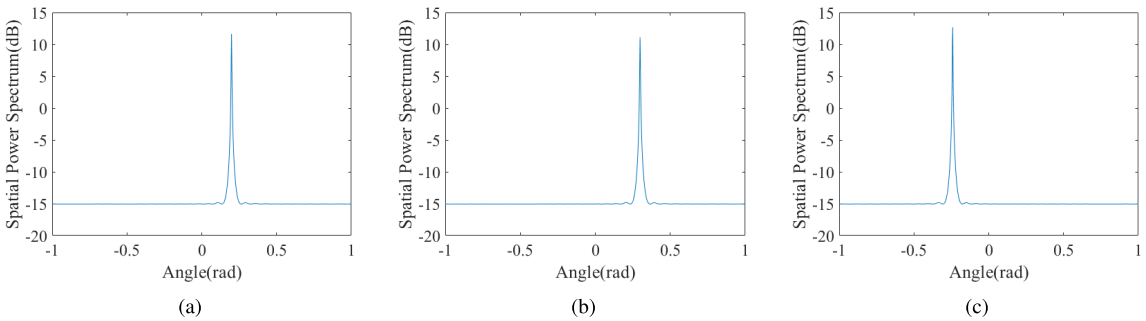

FIGURE 11. DoA estimation result of labeled targets (a) 1 (b) 2 (c) 3.

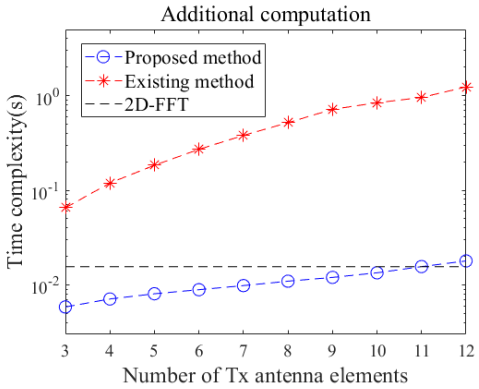

FIGURE 12. Time complexity comparison.

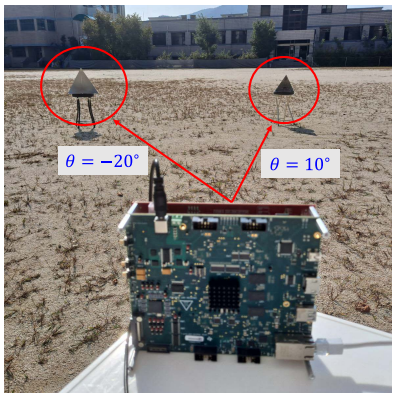

FIGURE 13. Experiment with two corner reflecters.

eigenvector corresponding to the biggest eigenvalue, the rest of eigenvectors represent the noise space. By investigating the Euclidean distance between the steering vector and the noise space (E_{N}) [23], we obtain the spatial power spectrum. That is,

$$P_{\mathrm{MU}}(\theta) = \frac{1}{a(\theta)E_{\mathrm{N}}^{\mathrm{H}}E_{\mathrm{N}}a(\theta)^{\mathrm{H}}}, \tag{23}$$

where the steering vector $a(\theta)$ is defined as

$$a(\theta) = \left[1, e^{\frac{d\sin(\theta)}{\lambda}}, e^{\frac{2d\sin(\theta)}{\lambda}}, \cdots, e^{\frac{(N_{\mathrm{Tx}}N_{\mathrm{Rx}}-1)d\sin(\theta)}{\lambda}}\right]. \tag{24}$$

By investigating the maximum value of P_{MU} for each labeled target, the corresponding angle will be the estimated DoA. Note that angles for each target were set to be $(0.2, -0.24, 0.3)$. Angle estimation results for each labeled target are shown in Fig. 11.

V. IMPLEMENTATION

A. IMPLEMENTATION ISSUES OF THE PROPOSED SCHEME

Conditions for the proposed MPSK code: we need two conditions for the MPSK code. Since we are dealing with the discrete beat signals, $M\phi_i$ must be integer value for all $i = 0, \cdots, N_{\mathrm{Tx}} - 1$. Second, since we use inverse matrix of the circulant matrix A of the MPSK code, it must be invertible. For example, if the set of MPSK code of $\{0, 1/4, 2/4, 3/4\}$ is applied to the Tx antenna array with $N_{\mathrm{Tx}} = 4$ as in [22], true target peaks cannot be found since the circulant matrix of the MPSK code is not invertible. Therefore, the MPSK code with invertible circulant matrix must be designed. Fortunately, the rank of the circulant matrix defined in Equation 13 is known to be $\gcd(f(x), x^n - 1)$ [31], where $f(x) = \sum_{i=0}^{M-1} a_i x^i$. Once the MPSK code is decided, the rank of the circulant matrix of the MPSK code can be easily calculated by the polynomial remainder theorem [32] and we can choose the MPSK code which makes the circulant matrix invertible.

Complexity analysis: Compared to the TDM MIMO scheme regarding to the computational complexity, the main overhead for the proposed scheme is matrix inversion in (16). We could lower the complexity of the matrix inversion by using the diagonalization property of the circulant matrix. The circulant matrix inversion using FFT has the complexity of $O(M \log M)$ since it is multiplied by each row of Index_peak1(I_1), it has a total complexity of $O(MN \log M)$. As 2D-FFT for the R-v domain has the complexity of $O(MN \log(MN))$, the proposed method does not significantly affect the complexity of radar processing.

Furthermore, the time complexity of the proposed method and the existing method in [21] was compared. Since the method in [21] requires the DoA estimation for all virtual arrays, a large amount of computation is required for the separation of Tx signals. However, the proposed method does

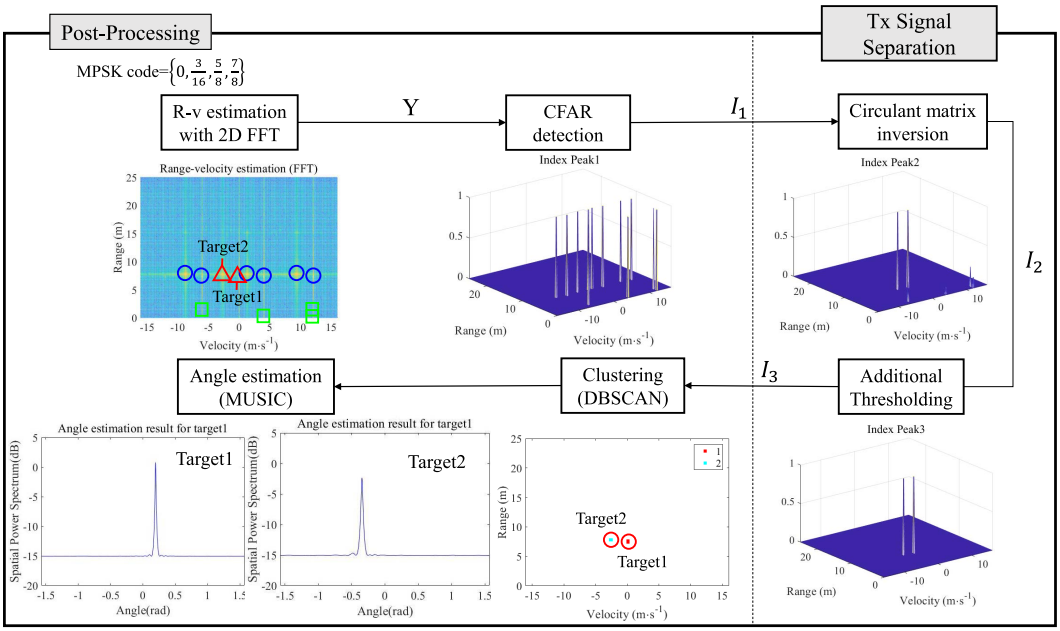

FIGURE 14. Implementation of the proposed scheme with commercial radar.

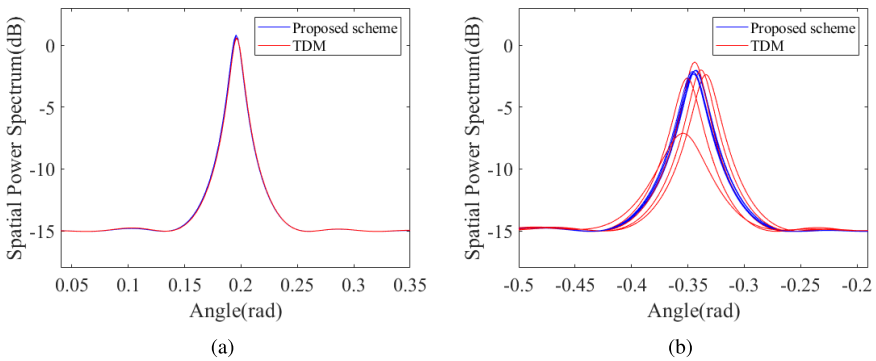

FIGURE 15. Angle estimation performance of TDM vs proposed method for (a) the static target (b) the moving target.

not require this step. Instead, it requires circulant matrix inversion only once to find true peaks and to configure a virtual array. In Fig. 12, the additional processing time to separate Tx signals according to N_{Tx} are compared by the simulation under the matlab 2019.b environment with CPU i5-9600k. It shows that the proposed method has superb gain in aspect of the time complexity.

B. EXPERIMENT

To evaluate the proposed scheme, MMWCAS-RF-EVM from Texas Instrument, which is a cascade of 4 AWR2243 FMCW radar chips was used. AWR2243 is composed of 3×4 MIMO, and a total of 12×16 antenna array by cascading 4 AWR2243 radar chips are exploited to enhance the angle estimation performance. Among the antenna array, 4×8 ULA antennas with Tx antenna element spacing 4λ and Rx antenna element spacing $\lambda/2$ were used for the experiment. AWR2243 provides a phase shift function for beam-forming, and we used this function to apply different phase shift per chirps to implement the proposed multiplexing scheme.

Fig.13 shows the experiment configuration with two corner reflectors as targets. The first target was placed in front of the radar at (10)-degree position from the normal direction with distance 7.5m, and the second target was placed at (-20)-degree position with distance 8m. The first corner target was stationary, and the other corner reflector was moved in the direction toward the radar. Radar parameters for the experiment are in Table. 2 as same as the simulation in section IV. Step by step results are shown in Fig. 14. Red, blue, and green circles indicate real target peaks, ghost target peaks due to the MPSK code, and the peak due to self-interference or ground clutters, respectively.

Furthermore, an additional experiment was conducted to compare the conventional TDM scheme and the proposed

scheme. Along with the advantage of resolving the velocity ambiguity problem, the proposed scheme showed higher SNR properties compared to the conventional TDM scheme. The peak of the first target for the proposed scheme showed 12.9dB higher peak power on average. This result coincides with the theoretical 12dB ($\approx 10\log_{10}(N_{\mathrm{Tx}})$) SNR gain which can be obtained by using all of the time slots.

In addition, the proposed scheme showed a more accurate angle estimation performance compared to the TDM MIMO scheme. For each scheme, a total 5 frames were captured and radar parameters were set to be identical. As shown in Fig. 15, the angle estimation result of the static target showed stable performance for both schemes. However, the TDM scheme showed unstable angle estimation performance for the moving target. Since the TDM scheme requires phase calibration of the moving target for each Tx signal [14], inaccurate estimation of the target's velocity leads to angle estimation performance degradation.

VI. CONCLUSION

In this paper, we propose a novel multiplexing scheme for MIMO radar using specific MPSK code and corresponding post-processing steps to resolve the velocity ambiguity problem. The proposed scheme includes the circulant matrix inversion to find the true target peaks among the detected peaks, which is computationally efficient. Consequently, the proposed scheme was successfully implemented by the state-of-the-art commercial radar regardless of phase distortion issues which was major problem in the previous method.

In addition, the proposed multiplexing scheme showed various advantages compared to the conventional TDM scheme in the aspect of SNR and angle estimation performance for moving targets. We hope that this scheme could alleviate several issues in the conventional TDM scheme while resolving the velocity ambiguity problem and enables more exact estimation of the target's 4D information.

REFERENCES

[1] S. M. Patole, M. Torlak, D. Wang, and M. Ali, "Automotive radars: A review of signal processing techniques," *IEEE Signal Process. Mag.*, vol. 34, no. 2, pp. 22–35, Mar. 2017.

[2] J. Hatch, A. Topak, R. Schnabel, T. Zwick, R. Weigel, and C. Waldschmidt, "Millimeter-wave technology for automotive radar sensors in the 77 GHz frequency band," *IEEE Trans. Microw. Theory Techn.*, vol. 60, no. 3, pp. 845–860, Mar. 2012.

[3] S. Campbell, N. O'Mahony, L. Krpalcova, D. Riordan, J. Walsh, A. Murphy, and C. Ryan, "Sensor technology in autonomous vehicles: A review," in *Proc. 29th Irish Signals Syst. Conf. (ISSC)*, Jun. 2018, pp. 1–4.

[4] Z. Feng, S. Zhang, M. Kunert, and W. Wiesbeck, "Point cloud segmentation with a high-resolution automotive radar," in *Proc. 10th AmE Automotive Meets Electron. GMM-Symp.*, 2019, pp. 1–5.

[5] O. Schumann, M. Hahn, J. Dickmann, and C. Wöhler, "Semantic segmentation on radar point clouds," in *Proc. 21st Int. Conf. Inf. Fusion (FUSION)*, Jul. 2018, pp. 2179–2186.

[6] B. Kim, S. Kim, and J. Lee, "A novel DFT-based DOA estimation by a virtual array extension using simple multiplications for FMCW radar," *Sensors*, vol. 18, no. 5, p. 1560, May 2018.

[7] S. Sun, A. P. Petropulu, and H. V. Poor, "MIMO radar for advanced driver-assistance systems and autonomous driving: Advantages and challenges," *IEEE Signal Process. Mag.*, vol. 37, no. 4, pp. 98–117, Jul. 2020.

[8] H. Sun, F. Brigui, and M. Lesturgie, "Analysis and comparison of MIMO radar waveforms," in *Proc. Int. Radar Conf.*, Oct. 2014, pp. 1–6.

[9] J. Guetlein, A. Kirschner, and J. Detlefsen, "Calibration strategy for a TDM FMCW MIMO radar system," in *Proc. IEEE Int. Conf. Microw., Commun., Antennas Electron. Syst. (COMCAS)*, Oct. 2013, pp. 1–5.

[10] A. J. Duly, D. J. Love, and J. V. Krogmeier, "Time-division beamforming for MIMO radar waveform design," *IEEE Trans. Aerosp. Electron. Syst.*, vol. 49, no. 2, pp. 1210–1223, Apr. 2013.

[11] J. J. M. de Wit, W. L. van Rossum, and A. J. de Jong, "Orthogonal waveforms for FMCW MIMO radar," in *Proc. IEEE RadarCon (RADAR)*, 2011, pp. 686–691, doi: 10.1109/RADAR.2011.5960625.

[12] S. Hamidi and S. S. Naeini, "CDM based virtual FMCW MIMO radar imaging at 79 GHz," in *Proc. IEEE Can. Conf. Electr. Comput. Eng. (CCECE)*, Sep. 2021, pp. 1–4.

[13] R. Feger, C. Pfeffer, and A. Stelzer, "A frequency-division MIMO FMCW radar system based on delta–sigma modulated transmitters," *IEEE Trans. Microw. Theory Techn.*, vol. 62, no. 12, pp. 3572–3581, Dec. 2014.

[14] (2021). *RETINA The Smart 4D Image Radar*. [Online]. Available: https://www.smartradarsystem.com/retina

[15] (2020). *MMWCAS-RF-EVM mmWave Cascade Imaging Radar RF Evaluation Module*. [Online]. Available: https://www.ti.com/tool/MMWCAS-RF-EVM

[16] (2021). *Vayyar Releases World's First MIMO Single-Chip 'XRR' RFIC With 48 Transceivers and on-Chip Processing*. [Online]. Available: https://blog.vayyar.com/xrr-0-300-m-single-chip

[17] M. Kronauge, C. Schroeder, and H. Rohling, "Radar target detection and Doppler ambiguity resolution," in *Proc. 11th Int. Radar Symp.*, Jun. 2010, pp. 1–4.

[18] T. R. Tuinstra, "Range and velocity disambiguation in medium PRF radar with the DBSCAN clustering algorithm," in *Proc. IEEE Nat. Aerosp. Electron. Conf. (NAECON) Ohio Innov. Summit (OIS)*, Jul. 2016, pp. 396–400.

[19] F. Roos, J. Bechter, N. Appenrodt, J. Dickmann, and C. Waldschmidt, "Enhancement of Doppler unambiguity for chirp-sequence modulated TDM-MIMO radars," in *IEEE MTT-S Int. Microw. Symp. Dig.*, Apr. 2018, pp. 1–4.

[20] Y. L. Sit, G. Li, S. Manchala, H. Afrasiabi, C. Sturm, and U. Lubbert, "BPSK-based MIMO FMCW automotive-radar concept for 3D position measurement," in *Proc. 15th Eur. Radar Conf. (EuRAD)*, Sep. 2018, pp. 289–292.

[21] H. Sim, S. Kang, S. Lee, and S. Kim, "Improved DOA estimation method by distinction of different transmit signals in automotive MIMO frequency-modulated continuous wave radar systems," *IET Radar, Sonar Navigat.*, vol. 14, no. 8, pp. 1135–1142, Aug. 2020.

[22] J. Jung, S. Lim, S.-C. Kim, and S. Lee, "Solving Doppler-angle ambiguity of BPSK-MIMO FMCW radar system," *IEEE Access*, vol. 9, pp. 120347–120357, 2021.

[23] R. O. Schmidt, "Multiple emitter location and signal parameter estimation," *IEEE Trans. Antennas Propag.*, vol. AP-34, no. 3, pp. 276–280, Mar. 1986.

[24] A. M. Elbir, "DeepMUSIC: Multiple signal classification via deep learning," *IEEE Sensors Lett.*, vol. 4, no. 4, pp. 1–4, Apr. 2020.

[25] H. Rohling, "Ordered statistic CFAR technique—An overview," in *Proc. 12th Int. Radar Symp. (IRS)*, Sep. 2011, pp. 631–638.

[26] G. Minkler and J. Minkler, *CFAR: The Principles of Automatic Radar Detection in Clutter*. Baltimore, MD, USA: Magellan Book Co., 1990, p. 384.

[27] M. A. Richards, *Fundamentals of Radar Signal Processing*. New York, NY, USA: McGraw-Hill, 2014.

[28] R. Gray, "Toeplitz and circulant matrices: A review," *Found. Trends Commun. Inf. Theory*, vol. 2, no. 3, pp. 155–239, 2006.

[29] H. J. Nussbaumer, "The fast Fourier transform," in *Fast Fourier Transform and Convolution Algorithms*. Cham, Switzerland: Springer, 1981, pp. 80–111.

[30] M. Ester, H. P. Kriegel, J. Sander, and X. Xu, "A density-based algorithm for discovering clusters in large spatial databases with noise," in *Proc. 2nd Int. Conf. Knowl. Discovery Data Mining*, Portland, OR, USA, Aug. 1996, vol. 96. no. 34, pp. 226–231.

[31] A. W. Ingleton, "The rank of circulant matrices," *J. London Math. Soc.*, vol. 1, no. 4, pp. 445–460, 1956.

[32] C. Clapham, J. Nicholson, and J. R. Nicholson, *The Concise Oxford Dictionary of Mathematics*. London, U.K.: Oxford Univ. Press, 2014.

JEONG-HOON PARK (Graduate Student Member, IEEE) received the B.S. degree in electrical and computer engineering from Seoul National University, Seoul, South Korea, in 2020, where he is currently pursuing the Ph.D. degree. His current research interests include radar signal processing techniques and joint radar-communication systems.

YOUNG-JUN YOON (Graduate Student Member, IEEE) received the B.S. degree in electrical and computer engineering from the University of Seoul, Seoul, Republic of Korea, in February 2015. He is currently pursuing the Ph.D. degree with Seoul National University, Seoul. His research interests include cover signal processing for security of wireless communication systems, radar signal processing, and deep machine learning application for communications.

JAEHOON JUNG (Graduate Student Member, IEEE) received the B.S. degree in electrical and computer engineering from Seoul National University, Seoul, Republic of Korea, in 2018, where he is currently pursuing the Ph.D. degree. His research interests include radar signal processing techniques, especially on automotive radar systems.

SEONG-CHEOL KIM (Senior Member, IEEE) received the B.S. and M.S. degrees in electrical engineering from Seoul National University, Seoul, South Korea, in 1984 and 1987, respectively, and the Ph.D. degree in electrical engineering from the Polytechnic Institute, New York University (NYU), Brooklyn, NY, USA, in 1995. From 1995 to 1999, he was with the Department of Wireless Communications Systems Engineering, AT&T Bell Laboratories, Holmdel, NJ, USA. Since 1999, he has been a Professor with the Department of Electrical and Computer Engineering, Seoul National University. His research interests include wireless communication systems, including millimeter-wave channel modeling, wireless localization systems, acoustic channel modeling, wireless channel measurements, and automotive radar signal processing.